

Observing dynamical localization on a trapped-ion qudit quantum processor

Gonzalo Camacho,^{1,*} Claire L. Edmunds,² Michael Meth,² Martin Ringbauer,² and Benedikt Fauseweh^{1,3}

¹*Institute of Software Technology, German Aerospace Center (DLR),
Rathausallee 12, 53757 Sankt Augustin, Germany*

²*Institut für Experimentalphysik, University of Innsbruck, Technikerstraße 25, 6020 Innsbruck, Austria*

³*Department of Physics, TU Dortmund University, Otto-Hahn-Str. 4, 44227 Dortmund, Germany*

The advancements of quantum processors offer a promising new window to study exotic states of matter. One striking example is the possibility of non-ergodic behaviour in systems with a large number of local degrees of freedom. Here we use a trapped-ion qudit quantum processor to study a disorder-free $S = 1$ Floquet model, which becomes prethermal by dynamic localization due to local spin interactions. We theoretically describe and experimentally observe an emergent $3T$ subharmonic response, demonstrating the ability to witness non-ergodic dynamics beyond qubit systems. Our numerical simulations reveal the role played by multipartite entanglement through the Quantum Fisher Information, showing how this quantity successfully reflects the transition between ergodic and localized regimes in a non-equilibrium context. These results pave the way for the study of ergodicity-breaking mechanisms in higher-dimensional quantum systems.

I. INTRODUCTION

Periodically driven quantum systems open a vast landscape to explore the emergence of distinct non-equilibrium phases of matter [1–4]. In addition, they also pose some of the most fundamental and challenging questions in understanding emergent physical phenomena in many-body systems. An isolated, periodically driven quantum system tends to absorb energy from the drive following the time evolution of the initial state. As a consequence, subregions of the system that can be locally probed are expected to evolve towards an effective infinite temperature state with trivial correlations [5–7]. This idea is captured by the Eigenstate Thermalization Hypothesis [8, 9] (ETH), which argues that generic quantum systems undergoing unitary evolution for sufficiently long times can eventually be well described by classical statistical ensembles [10]. In such scenario, all knowledge about the initial conditions of the system is ultimately lost. Thus, systems satisfying the ETH are often termed ergodic.

In the current fast-paced development of quantum information processing, identifying quantum states that coherently preserve local information is of interest to prevent such generic fate. Therefore, there has been growing interest to find exceptions to the ETH in systems whose unitary dynamics exhibit a collective behavior rather resembling that of integrable or non-interacting systems. The most prominent example of systems undergoing weak ergodicity-breaking mechanisms in their unitary dynamics are many-body scarred states [11–17]. In these systems, the preparation of special highly-excited initial states and subsequent evolution in a disorder-free landscape results in long lived revivals of the initial state configuration.

In a different context, following Anderson’s seminal

work on localization for non-interacting particles [18], atypical thermalizing behavior has been reported to exist in highly disordered quantum lattices hosting local interactions, an emergent process known as many-body localization (MBL) [19–21]. Much effort has been devoted to merging these scenarios with the goal of exploring systems featuring unconventional quantum many-body dynamics. A particularly exciting scenario occurs when both periodic driving and MBL are combined, since the existence of emergent local symmetries in the MBL phase leads to an exponentially slow heating mechanism when the system absorbs energy from the drive [22]. Additionally, if a discrete time symmetry of the drive is spontaneously broken, an MBL discrete time crystal (MBL-DTC) [23, 24] emerges as a genuine non-equilibrium phase of quantum matter, characterized by a robust subharmonic response of spatio-temporal correlations. Experimental observations of the MBL-DTC phase [25, 26] have been replicated recently on quantum computers [27–29], further motivating the use of quantum hardware in the quest to identify genuine non-equilibrium quantum states able to coherently preserve quantum information up to very long time scales. In this direction, periodically driven models based on Floquet engineering have recently received considerable attention after being experimentally realized in both ordered [30, 31] and disordered [32–34] dipolar spin ensembles, constituting a current topic of interest in the use of digital quantum computers to simulate many-body quantum systems [35]. However, the experimental realization of MBL systems on current quantum processors comes at the cost of including strong disorder sampling, which ultimately leads to averaging over a vast number of configurations, introducing a large overhead.

An alternative approach to address periodically driven systems on current quantum computers is to explore clean (disorder-free) systems. Under certain nontrivial constraints, ergodicity-breaking dynamics can emerge as a collective response of the system to periodic driving, leading to an overall dynamical localization effect that

* gonzalo.camacho@dlr.de

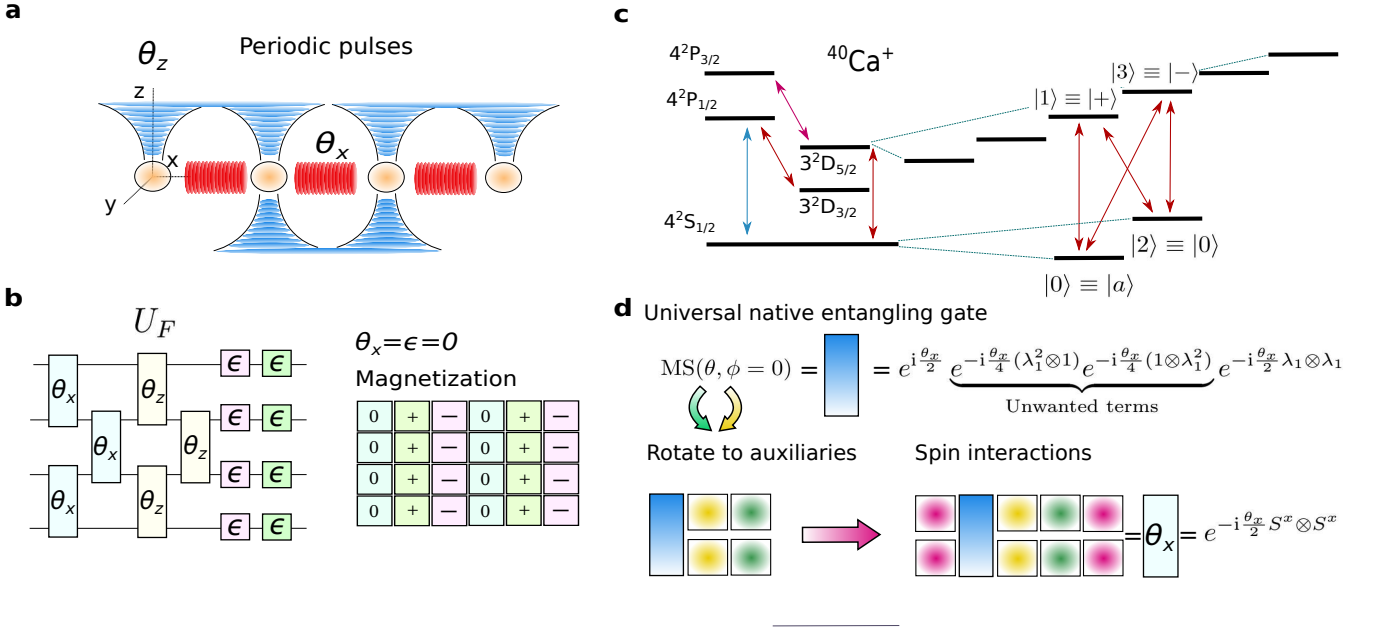


FIG. 1. **a** Schematic representation of periodic pulses on a chain of trapped ions by alternating couplings θ_x, θ_z in the x and z directions of the ions, respectively. **b** The corresponding circuit realization for a digital quantum gate implementation of the Floquet unitary operator U_F studied in this work. The kick parameter θ_x represents the strength of the entangling gates along the x directions of spins, followed by a layer of entangling gates acting along the z components of the spins depending on the parameter θ_z . A set of local rotations represented by P_ϵ^{z3} in Eq. (1) follow the entangling gates. If both $\epsilon = \theta_x = 0$, any initial product state in the z basis of spins becomes an eigenstate of U_F^3 , thus featuring a 3-periodic pattern in the magnetization; in the example, the initial state is $|\Psi_0\rangle = |0\rangle^{\otimes L}$ for a chain of $L = 4$ spins. A finite value of θ_x will destabilize the perfectly oscillating pattern of the magnetization $\langle S^z \rangle$; employing entangling gates along the z direction right after the kicks along the x direction contributes to restore the oscillations. **c** Implementation of spin-spin interactions in the $^{40}\text{Ca}^+$ trapped-ion qudit quantum processor of Ref. [36], schematically showing the ion energy levels. The encoding of a single spin-1 into a four-dimensional space with basis states $|a\rangle, |+\rangle, |0\rangle, |-\rangle$ is sketched, along with the addressed transitions needed; note that our trapped-ion device can access more transitions between levels which are not represented here. **d** The universal entangling gate $\text{MS}(\theta, \phi = 0)$ contains unwanted local terms that can be isolated into the auxiliary level $|a\rangle$ of the encoding employing appropriate local rotations (Different rotation angles have been represented by different colors, see Appendix 1 for details). Isolation of unwanted local phases into the auxiliary levels allows to engineer spin-spin interacting gates for the Floquet operator U_F .

potentially survives in the thermodynamic limit [37, 38]. This generally occurs if the driving frequency is large compared to the characteristic frequency scales of the system, precluding the system from readjusting its interlevel transitions at every cycle, translating into exponentially long heating times having well defined, rigorous bounds [39]. The consequence of this clear separation of energy scales is the appearance of a prethermal phase [40–44] that will resemble equilibrium way beyond the coherence times of the system before heating effects break in.

In this work, we investigate an $S = 1$ Floquet model whose unitary evolution operator induces a robust dynamical localization effect for a translation invariant initial state. The existence of dynamical localization in the model is verified by experiments carried out on a trapped-ion qudit quantum processor [36]. By focusing on spatio-temporal correlations and the dynamics of entanglement, we perform further numerical simulations of the model to explore the non-equilibrium phase diagram,

demonstrating that coherent evolution retains knowledge of the initial state up to very long time scales, with the state reaching a prethermal phase.

II. MODEL AND EXPERIMENTAL REALIZATION

We consider a one dimensional chain of L spins with spin value $S = 1$ interacting to nearest neighbors; unless otherwise stated, we employ open boundary conditions throughout this work, and use units of $\hbar = 1$. As a local basis, we choose the eigenstates of the S^z spin component, given by $\{|+\rangle, |0\rangle, |-\rangle\}$. The initial state is chosen to be $|\Psi_0\rangle = |0\rangle^{\otimes L}$. The state is subject to unitary evolution, which introduces interactions between neighbouring spins in the lattice by applying consecutive periodic pulses in the x and z directions, as sketched in Fig. 1a. The periodic evolution of the state employs a ternary Floquet drive, represented by a unitary operator U_F given

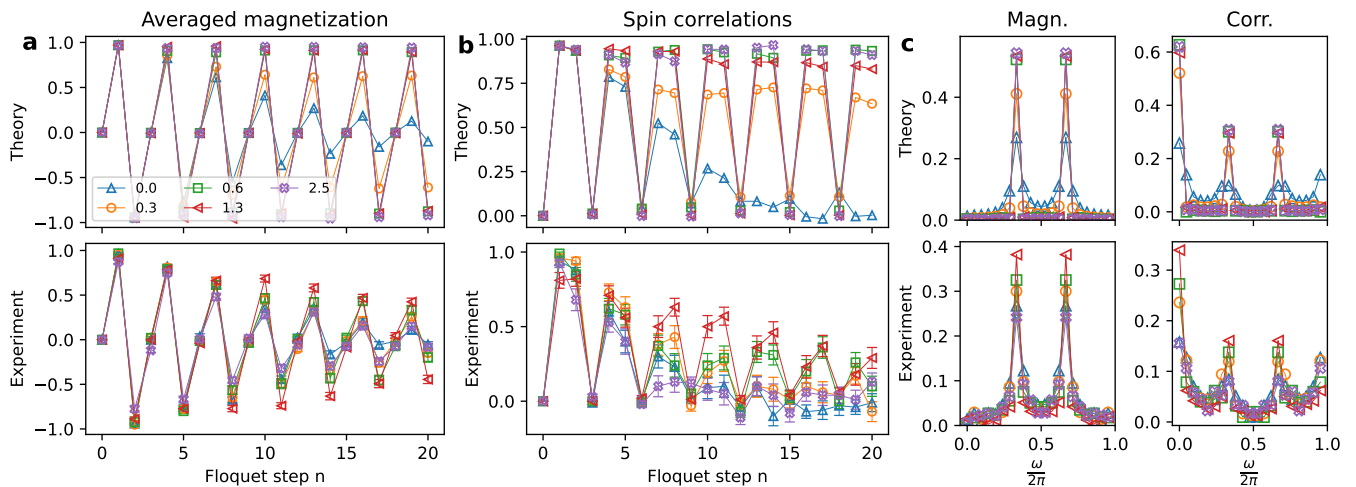


FIG. 2. Comparison between theory and experiment results obtained in the trapped-ion qudit device of Ref. [36] for a chain of $L = 4$ spins, with $\theta_x = 0.2$ and a total of 20 Floquet steps, for different values of θ_z as indicated in the legend. Error bars corresponding to one standard deviation have been included in the experimental data, and are calculated using Monte Carlo resampling. **a** The spatially averaged magnetization, showing the survival of oscillations with increasing value of θ_z , signalling the appearance of dynamical localization. Note that the behaviour with increasing θ_z is consistent between experiment and theory, with the exception of $\theta_z = 2.5$, which we attribute to gate errors. **b** The spin correlations along the z direction for two neighbouring spins in the chain get enhanced with increasing value of θ_z . **c** Discrete Fourier Transform representation to frequency domain for the magnetization and spin correlations from Figs. **a** and **b**. The appearance of peaked values in the Fourier spectrum at $\omega = \frac{2\pi}{3}, \frac{4\pi}{3}$ indicates the emergence of subharmonic response to the external drive.

by

$$\begin{aligned}
 U_F &= P_\epsilon^{\mathbb{Z}_3} e^{-i\frac{\theta_x}{2} \sum_{j=1}^{L-1} S_j^z S_{j+1}^z} e^{-i\frac{\theta_z}{2} \sum_{j=1}^{L-1} S_j^x S_{j+1}^x} \\
 &= P_\epsilon^{\mathbb{Z}_3} U_x U_z, \\
 P_\epsilon^{\mathbb{Z}_3} &= \prod_{j=1}^L e^{-i\frac{\pi-\epsilon}{2} \lambda_{6,j}} \prod_{j=1}^L e^{-i\frac{\pi-\epsilon}{2} \lambda_{1,j}}. \quad (1)
 \end{aligned}$$

A digital circuit implementation of this Floquet unitary operator is represented in Fig. 1b. The matrices $\lambda_{1,j}, \lambda_{6,j}$ represent the first and sixth Gell-Mann matrices at site j of the chain, respectively (following the notation of Ref. [36]).

The first two contributions of the drive, U_x and U_z , consist of uniform spin-spin interactions between neighbouring sites, first with U_x acting along the x direction of the spins, and then with U_z acting along the z direction. The parameters θ_x, θ_z represent the duration of the interaction pulses between the spins, which is scaled by the characteristic time scale of the uniform interactions. We note that the interacting terms along the x and z directions are related to each other by a unitary transformation, but $[U_x, U_z] \neq 0$. The $P_\epsilon^{\mathbb{Z}_3}$ term of the drive generates a set of local rotations, and contains a discrete \mathbb{Z}_3 symmetry in the case $\epsilon = 0$, with level transitions given by $|0\rangle \rightarrow |+\rangle, |+\rangle \rightarrow |-\rangle, |-\rangle \rightarrow |0\rangle$; for $\epsilon = \pi$, the \mathbb{Z}_3 symmetry in $P_{\epsilon=\pi}^{\mathbb{Z}_3} = \hat{1}$ is absent. In what follows, and unless otherwise stated, we will focus on the case $\epsilon = 0$. If both $\epsilon = \theta_x = 0$, any initial product state in the $\{|+\rangle, |0\rangle, |-\rangle\}$ basis is an eigenstate of U_F^3 , and $|\langle \Psi_0 | U_F^{3n} | \Psi_0 \rangle|^2 = 1$ for any $n \in \mathbb{N}$, see Fig. 1b. For finite

$\theta_x > 0$ values, the system is coupled to the set of non-uniform states in the z basis, which can be interpreted as a bath for the spin-1 system. We note that the total magnetization along the z direction of spin, $\sum_j S_j^z$, is not a conserved quantity in this model. We implement the model on a trapped-ion qudit quantum processor [36], where the spins of the chain are encoded as a *qudit*, i.e. three level quantum systems. We refer to Figs. 1c, d, and Appendix 1 for details on the encoding procedure.

III. RESULTS

A. Robust subharmonic oscillations

We characterize the emergence of spatio-temporal order in the system dynamics by measuring the averaged magnetization across all spins of the chain and the spin correlations between spins located at different lattice sites. Figure 2 shows the experimental results for a small chain of $L = 4$ spins, compared to the theory prediction for a fixed parameter θ_x along the x direction of spin interactions and for different values of the θ_z parameter. Our experimental results verify that increasing values of θ_z , i.e. stronger interaction between neighbouring spins along the z -direction, lead to the stabilization of the subharmonic response in the system, which otherwise quickly decays in the case of $\theta_z = 0$. The fact that finite θ_z values following a kick with $\theta_x \neq 0$ restore the appearance of robust 3-periodic oscillations is a signature of dynamical

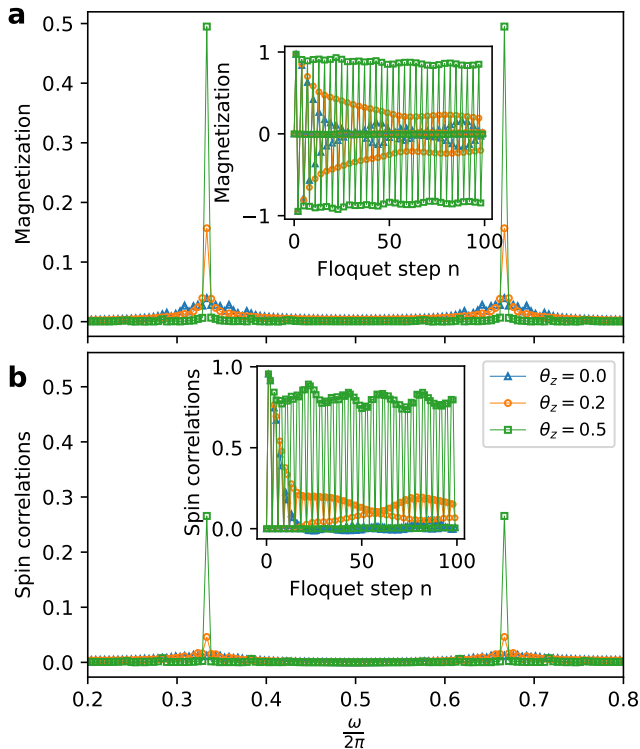


FIG. 3. Exact time evolution simulation for a chain of $L = 12$ spins with $\epsilon = 0$, $\theta_x = 0.2$ and a total of $n = 200$ Floquet steps. **a** Fourier transform of the spatially averaged magnetization (see Supplemental Information for a precise definition of these observables); the insets represent the time evolution for each observable for the first 100 steps of the evolution. **b** Fourier transform of the spin-spin correlations in the z direction between the middle chain spin and the right-most edge one. Both observables feature robust 3-periodic oscillations with increasing θ_z values.

cal localization in the system away from the trivial point $\theta_x = 0$. The enhanced subharmonic response for finite θ_x is more clearly visualized in Fig. 2c, where the Fourier representation of the associated time signal shows peaked values at frequencies $\frac{\omega}{2\pi} = 1/3, 2/3$.

To verify the survival of these oscillations with increasing system size, and to rule out that the observed effect is solely due to revivals in the small system, we have complemented the results from Fig. 2 with numerical simulation results for a chain of $L = 12$ spins in Fig. 3. We conclude that both the magnetization and spin correlations experience a robust subharmonic response with increasing values of θ_z in larger system sizes, as evidenced by their representation in Fourier space. The persistence of subharmonic oscillations in the system is verified in the thermodynamic limit by exploiting the translational invariance of the system (see Appendix 2).

B. Overlap and bipartite entanglement phase diagrams

In order to explore the general behavior of the system for a wide range of variations in the θ_x, θ_z parameters, we have represented the phase diagram for the averaged overlap of the time evolved state with the initial state and the half-chain entanglement entropy in Fig. 4a, for a finite chain of size $L = 10$. In both cases, we observe two well differentiated regions: A region where unitary dynamics presents localized behavior featuring high overlap with the initial state and small bipartite entropy, with the system retaining knowledge of the initial conditions in the state; a region showing diffusive dynamics corresponding to low overlap and high entropy, where knowledge of the initial configuration is erased. In the latter region, the dynamics of the system is ergodic. Interestingly, we observe values of θ_z for which the ergodic phase is present for almost any finite $\theta_x > 0$; these values correspond to the dipped regions in Fig. 4a. An analytic identification of two of these points is possible employing a simple perturbative expansion for the parameter $\delta_x = \frac{\theta_x}{2}$, as explained in Appendix 3.

Results obtained in the trapped-ion experiment for the contrast change in the site-averaged magnetization are represented in Fig. 4b, with values of θ_z varying along the horizontal red line in Fig. 4a. The observed lifetime of the average magnetization oscillations serves as a proxy to identify and contrast emergent ergodic and localized regions in the dynamics of the system, with peak lifetime values indicating high probability to return to the initial configuration at every 3-periodic application of the unitary U_F . In the experiment, two concurrent effects occur. First, the decoherence of the device leads to a temporal loss of signal. Second, thermalization in the ergodic regime overlaps with this decoherence, making it difficult to distinguish between the two phenomena. Despite these challenges, it is clearly evident that the decay exhibits a strong dependence on the localization parameter θ_z . For values $\theta_z \sim 1.1$, the longest lifetimes are observed, in accordance with results from Fig. 4a. Importantly, the experiment clearly reproduces the predicted dipped region at $\theta_z \sim 2.1$, observed in the phase diagrams in Fig. 4a. This is followed by increased revivals of the initial states for $\theta_z > 2.1$, thus verifying the existence of a dynamically localized regime. We note that this revival is observable despite increasing gate errors with θ_z .

To further investigate the dependence with system size, we have represented the overlap and bipartite entanglement entropy in Figs. 4c for different values of the chain size L evolving the state up to very long time scales. We observe favourable scaling with L for the overlap with the initial state, which remains above 60% for $L = 12$ for a large number of cycles. This translates into a slow growth of the bipartite entropy $S_{L/2}$.

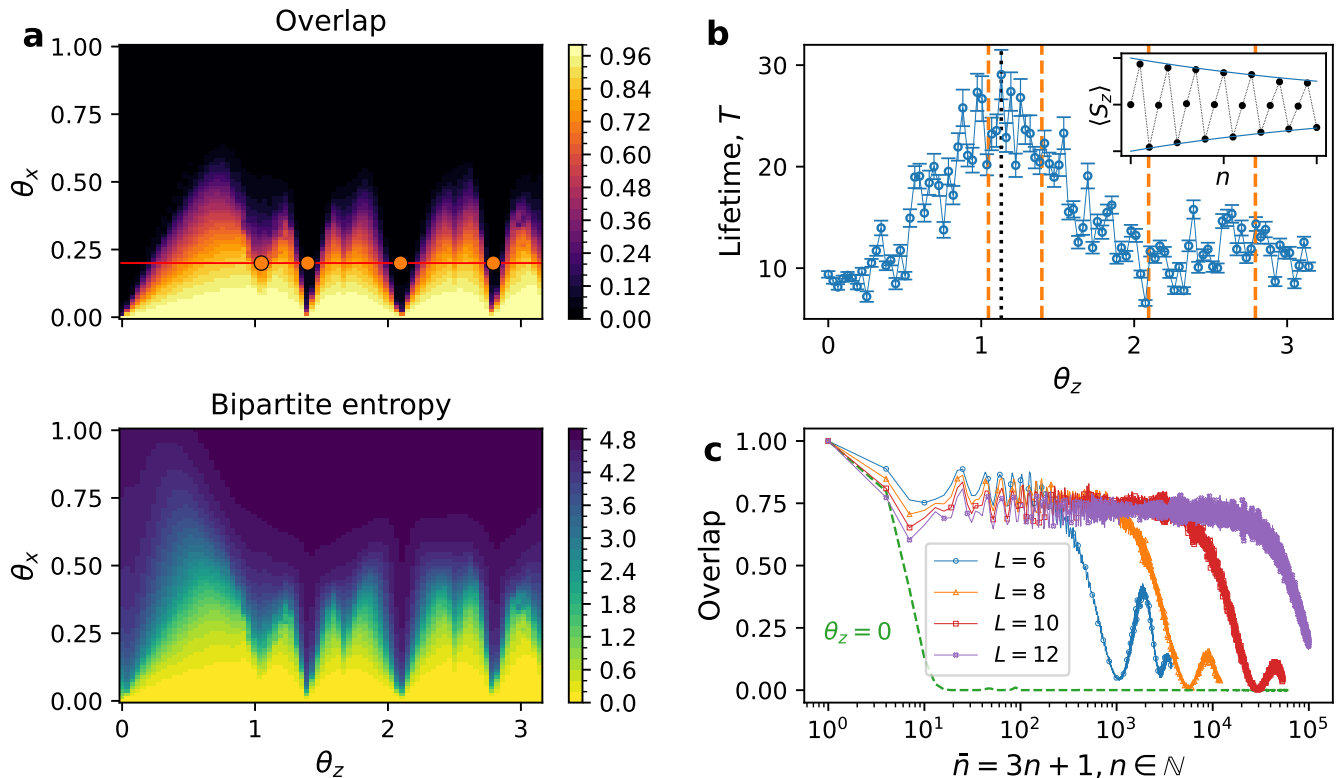


FIG. 4. **a** Phase diagrams for the overlap and the bipartite entanglement entropy for a chain of $L = 10$ spins, extracted from the exact time evolution of the state and averaged over a total of 500 Floquet cycles, represented as a function of the pulse angles θ_x, θ_z . The overlap is averaged at time steps $\bar{n} = 3n, n \in \mathbb{N}$. Note that times \bar{n} correspond to values $\mathcal{F} = 1$ for $\theta_x = 0$. The dark region indicates ergodic behavior in the system, whereas bright values indicate a high probability of return to the initially prepared product state, signaling a localized regime. Values of $\theta_z = \frac{4\pi}{9}, \frac{6\pi}{9}, \frac{8\pi}{9}$ are identified for which the behavior is ergodic (depth regions) almost at any value of $\theta_x > 0$ (see Appendix 3). Both phase diagrams show a one-to-one correspondence with each other. **b** Contrast change in the experimental averaged magnetization data shown in Fig. 2a. An exponential decay is fitted to the oscillation envelope to extract the lifetime T in units of Floquet steps, n : $e^{-n/T}$. Error bars correspond to one standard deviation calculated using Monte Carlo resampling. (Inset) An example of an exponentially decaying envelope fitted to the average magnetization $\langle S_z \rangle$, shown for $\theta_z = 1.1$, which corresponds to the maximum measured lifetime, $T = 29(2)$ (black dashed vertical line in main figure). The location of the dips represented by the colored filled dots in Fig. 4a correspond to the vertical dashed lines with matching color. **c** System size scaling for the overlap, with $\theta_x = 0.2, \theta_z = 0.5$ for different system sizes L ; the dashed curve corresponds to $\theta_z = 0, L = 10$. To include the point $n = 0$ in the logarithmic axis, data is represented against the shifted times $\bar{n} = 3n + 1$, corresponding to the times for which $\mathcal{F} = 1$ when $\theta_x = 0$; note that the initial point in the logarithmic x-axis at $\bar{n} = 1$ corresponds to the initial condition $n = 0$. For data visualization purposes, the curves corresponding to $\theta_z = 0.5$ have been represented only until times right after the overlap decays in value.

C. Multipartite entanglement non-equilibrium phase diagram

As a genuine multipartite entanglement witness, the Quantum Fisher Information (QFI) [45] has been shown to capture all relevant correlations leading to critical behavior for systems in thermal equilibrium, especially at zero temperature with ground states undergoing a quantum phase transition [46]. Along these lines, a question of interest is whether the QFI can play an analogous role in the non-equilibrium case, in particular concerning periodically driven systems that reach a prethermal phase.

Figure 5a shows the time-averaged scaled QFI f_Q phase diagram for a finite chain of $L = 10$ spins and a

range of values for the kick parameters θ_x, θ_z . We show that the QFI clearly traces the transition from ergodic to nonergodic regions previously shown in Fig. 4, and that both phase diagrams are in accordance with each other. In particular, we observe a critical region where the QFI gets maximized near the 4-partite entanglement upper bound; this occurs when $\theta_x \sim \theta_z$. This behavior of multipartite entanglement, where the QFI increases considerably at the boundaries separating the localized and ergodic regions suggests an interpretation of the QFI as a generalized susceptibility measure to characterize critical phenomena in periodically driven systems. To further complement these results, in Fig. 5b, we have represented the dynamics of f_Q for a fixed value of θ_x and three dif-

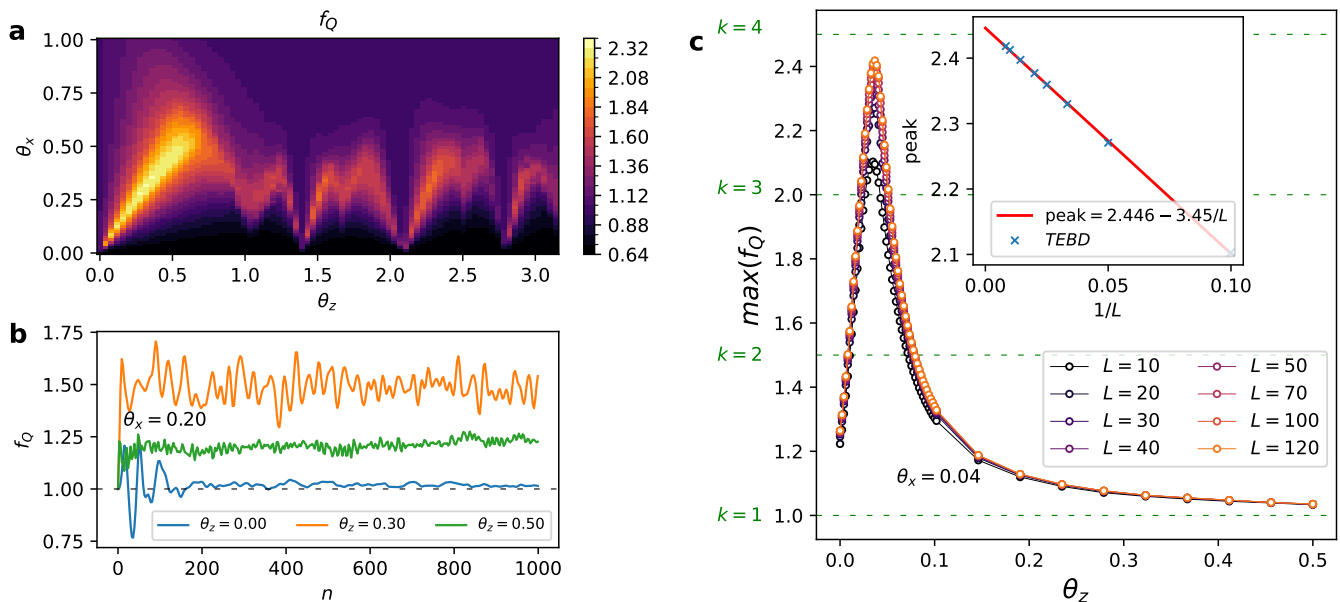


FIG. 5. **a** Non-equilibrium phase diagram for the QFI obtain through exact time evolution on a chain of $L = 10$ spin-1 spins, averaged over 500 Floquet cycles. The time-averaged QFI is enhanced at the boundaries in the crossover region separating the localized and ergodic regimes identified in Fig. 4a. **b** Time evolution of the QFI for fixed $\theta_x = 0.2$ at times $\bar{n} = 3n, n \in \mathbb{N}$. The dashed line indicates the upper bound in the QFI for separable states ($f_Q \leq 1$). **c** (Main panel) The maximum value of the QFI for a total of $n = 100$ Floquet cycles, with $\theta_x = 0.04$ using the time evolving block decimation (TEBD) with tolerance $\epsilon_{\text{TEBD}} = 10^{-6}$ for different system sizes L . The dashed horizontal lines represent different multipartite entanglement regions (with corresponding k -partite entanglement bounds represented by the dashed green lines), with $0.5 \leq f_Q \leq 1$ for separable states; the peak of f_Q is upper bounded by the 4-partite ($k = 4$) entanglement bound. **c** (Inset) The scaling with system size L of the peak in the QFI, showing the extrapolated value obtained in the $L \rightarrow \infty$ limit. The extrapolated result lies between the 3-partite and 4-partite upper bounds for entangled states (see the Supplementary Information for a definition of f_Q and its entanglement bounds).

ferent θ_z values, monitoring the evolution of the QFI at times $\bar{n} = 3n, n \in \mathbb{N}$, corresponding to the times where local rotations in the $\theta_x = 0$ case bring the state back to its initial preparation, up to a global phase. A key result is the observation that f_Q stabilizes to values corresponding to regions bounded by different multipartite entanglement sectors, and it does so within the time window plateau that identifies the duration of the prethermal phase in Fig. 4c. For $\theta_z = 0$, rapid thermalization occurs with the system showing multipartite entanglement. For finite θ_z values, dynamical localization locks the state to lie within different multipartite entanglement sectors. To further characterize the transition across the critical region witnessing maximal multipartite entanglement, in the main panel of Fig. 5c we have represented the maximum value for the QFI for a small value of the kick parameter θ_x , obtained from finite-size time-evolving block decimation (TEBD) simulations. We observe well-converged results at arbitrary θ_z values when approaching the thermodynamic limit by addressing larger system sizes L . The inset of Fig. 5c shows the scaling of the peak with respect to system size, extrapolating its value in the thermodynamic limit $L \rightarrow \infty$. In this limit, we obtain a value for the peak of ~ 2.446 , corresponding to a state between the 3-partite and 4-partite entanglement upper

bounds. This results are again in accordance with those of the phase diagrams shown in Fig. 4a. Based on these results, we conclude that the QFI stands as a valid proxy to probe the transition between regions corresponding to different dynamical phases in the non-equilibrium phase diagram.

IV. OUTLOOK

Dynamical localization in disorder-free quantum many-body systems stands as a prominent example of emergent, non-equilibrium phenomena and has recently gathered considerable attention using qubit-based quantum processors [47]. The results of this work exemplify the potential of employing qudit-based quantum computers for natively studying exotic quantum phenomena in systems where the number of local degrees of freedom exceeds those of conventional qubit-based processors.

The possibility of performing such experiments offers a unique opportunity to study systems like the one presented in this work, with great potential to unveil further anomalous thermalizing behavior existing in more general models. A fundamental understanding of the mechanism leading to dynamical localization in systems hosting

more local degrees of freedom than those based on conventional qubit-based models is highly desirable in this context and left open for future research. Since decoherence still poses a great obstacle in the realization of periodically driven systems in current digital quantum computers [27–29], correction methods based on quantum-classical feedback schemes [48] could potentially help improving the observation of periodic dynamics for longer times.

We comment on generalizations of the work presented here, arguing that models with higher spin degrees of freedom could potentially share similar collective behavior in their dynamics whenever the unitary evolution operator involves a discrete \mathbb{Z}_d symmetry, with $d = 2S + 1$ the local dimension associated to a system with spin value S . Another open question is to explore the stability of the observed oscillations and overlap revivals against finite values of the local kick parameter ϵ .

In addition to observing dynamical localization, our work emphasizes and demonstrates the key role played by multipartite entanglement witnesses in identifying collective non-equilibrium phenomena, which also has important implications in the context of quantum metrology [49]. Exploring multipartite entanglement dynamics poses a significant experimental challenge for future quantum simulators, but offers great potential for unveiling universal non-equilibrium features of many-body quantum systems [50]. For systems in thermal equilibrium, for instance, the QFI can be accessed experimentally [51] as a genuine witness of multipartite entanglement in quantum many-body systems showing critical behavior [46]. Our observations demonstrates a new connection between multipartite entanglement and non-equilibrium phase transitions between ergodic and non-ergodic dynamics. This connection opens a new pathway for analyzing the quantum dynamics of different (a priori unrelated) systems. A remarkable example along these lines is exploring the role played by the QFI in witnessing entanglement transitions in monitored random quantum circuits [52].

APPENDIX

1. Implementation on the qudit quantum processor

The native entangling gate of the qudit processor in Ref. [36] contains local terms that do not appear in the spin interactions present in the model (see [36] and the corresponding Supplementary Information for details). To get rid of these unwanted phases and being able to implement the spin-spin interactions in Eq. (1), we encode each qutrit into an extended Hilbert space of dimension 4, introducing an auxiliary degree of freedom that can be addressed by exploiting the allowed transitions between levels within a single ion, see Fig. 1c.

We define the encoding in a local basis $\{|a\rangle, |+\rangle, |0\rangle, |-\rangle\}$, where $|a\rangle$ represents the auxil-

iary level. The goal is to get rid of the local phases appearing in the native entangling gate [36]:

$$\text{MS}(\theta, \phi = 0) = e^{i\frac{\theta}{2}} e^{-i\frac{\theta}{4}(\lambda_1^2 \otimes 1)} e^{-i\frac{\theta}{4}(1 \otimes \lambda_1^2)} e^{-i\frac{\theta}{2}(\lambda_1 \otimes \lambda_1)}, \quad (2)$$

with λ_1 being the first Gell-Mann matrix. The native single qutrit gates can be expressed in terms of the Gell-Mann matrices as:

$$\begin{aligned} R_1(\theta, \phi) &= e^{-i\frac{\theta}{2}(\cos(\phi)\lambda_1 + \sin(\phi)\lambda_2)} = R_{+0}(\theta, \phi), \\ R_2(\theta, \phi) &= e^{-i\frac{\theta}{2}(\cos(\phi)\lambda_4 + \sin(\phi)\lambda_5)} = R_{+-}(\theta, \phi), \\ R_3(\theta, \phi) &= e^{-i\frac{\theta}{2}(\cos(\phi)\lambda_6 + \sin(\phi)\lambda_7)} = R_{0-}(\theta, \phi). \end{aligned} \quad (3)$$

In the extended Hilbert space for the qutrit encoding, we can define local rotation gates $Z_{ij}(\theta)$ between levels i, j . For example, between the $|+\rangle, |0\rangle$ states:

$$\begin{aligned} Z_{+0}(\theta) &= R_1(\pi/2, -\pi/2) R_1(\theta, 0) R_1(\pi/2, \pi/2) \\ &= \begin{pmatrix} 1 & 0 & 0 & 0 \\ 0 & e^{+i\frac{\theta}{2}} & 0 & 0 \\ 0 & 0 & e^{-i\frac{\theta}{2}} & 0 \\ 0 & 0 & 0 & 1 \end{pmatrix}. \end{aligned} \quad (4)$$

Thus, we can partially cancel the unwanted local terms as follows:

$$\begin{aligned} &\rightarrow \left[\underbrace{Z_{a+}(-\theta) Z_{+0}(-\theta/2)}_{\text{qutrit1}} \otimes \underbrace{Z_{a+}(-\theta) Z_{+0}(-\theta/2)}_{\text{qutrit2}} \right] \\ &\times \left[e^{i\frac{\theta}{2}} e^{-i\frac{\theta}{4}[(1 \otimes \lambda_1^2) + (\lambda_1^2 \otimes 1)]} e^{-i\frac{\theta}{2}(\lambda_1 \otimes \lambda_1)} \right] \\ &= e^{i\frac{\theta}{2}} A_1 A_2 e^{-i\frac{\theta}{2}(\lambda_1 \otimes \lambda_1)}, \end{aligned} \quad (5)$$

with A_1, A_2 being local operators acting on individual Hilbert spaces of qutrits 1 and 2, respectively, whose only non-trivial component belongs to the auxiliary level $|a\rangle$. Since the auxiliary level $|a\rangle$ does not couple under unitary dynamics to any other degrees of freedom, the unwanted phases will not affect the dynamics of the system. Alternatively, as the auxiliary rotations remove unwanted phases on qutrit sub-levels, they can also be replaced by phase tracking in software. In our work, we recorded the unwanted local phases on each qutrit level in software, and then updated the phases on all subsequent gates in the circuit to counteract the acquired phase. This approach is ideal to maximize fidelities across longer circuits.

This decomposition of the native gate allows to engineer spin-spin interactions in a simple way, by applying the appropriate local rotations to the exponential operator, transforming it to:

$$e^{i\frac{\theta}{2}} A_1 A_2 e^{-i\frac{\theta}{2}(\lambda_1 \otimes \lambda_1)} \xrightarrow{\text{local rotations}} \begin{cases} e^{-i\frac{\theta_x}{2} S^z \otimes S^z}, \\ e^{-i\frac{\theta_x}{2} S^x \otimes S^x}. \end{cases} \quad (6)$$

To this end, the following relations are useful:

$$\begin{aligned} R_2(\pi/2, \pi/2) \lambda_1 R_2^\dagger(\pi/2, \pi/2) &= S_x, \\ R_1(-\pi/2, +\pi/2) \lambda_1 R_1(-\pi/2, +\pi/2) &= \lambda_3. \end{aligned} \quad (7)$$

The exact form of the local rotations needed to transform the Gell-Mann matrices to spin-1 operators are described in detail in the Supplementary Information.

2. Quantum Fisher Information and numerical simulation details

The Quantum Fisher Information (QFI) for a pure state $|\psi\rangle$ and observable \mathcal{O} is given by:

$$\begin{aligned} F_Q[|\psi\rangle, \mathcal{O}] &= 4(\langle \mathcal{O}^2 \rangle - \langle \mathcal{O} \rangle^2), \\ \mathcal{O} &= \sum_i \mathcal{O}_i. \end{aligned} \quad (8)$$

As observables \mathcal{O} we choose each of the total angular momentum components across all chain sites $\hat{J}_{l=x,y,z} = \sum_{i=1}^L S_i^l$, for which the corresponding F_Q^l is calculated. The total QFI is defined as the sum over all components $F_Q = \sum_{l=x,y,z} F_Q^l$. For convenience, we work with the scaled quantity $f_Q = F_Q/8L$, since it allows for an easier visualization of the data compared against different multi-partite entanglement bounds (see Supplemental Information for details).

For finite chains up to $L = 12$ spins, the time evolution of the state is carried out employing sparse matrix-vector multiplications. For the QFI in Fig. 5c, we simulated the model employing the finite size TEBD algorithm [53], representing the operators as Matrix Product Operators (MPO). To address larger system sizes, we exploit the translational invariance of the model and employ the infinite version of the Time Evolving Block Decimation (iTEBD), keeping an error tolerance of $\varepsilon_{\text{TEBD}} = 10^{-6}$, allowing for dynamical increment of the bond dimension every time the error threshold is exceeded, stopping the simulation whenever the bond dimension $\chi > 600$.

3. Analytic estimation of the dips observed in the phase diagram

We carried out a perturbative treatment in the parameter $\delta_x = \frac{\theta_x}{2}$ in order to estimate the thermalization scales by direct analytical calculation in a finite chain system. Discarding all contributions of order $\mathcal{O}(\delta_x^2)$ and higher, after three consecutive applications of U_F over the initial state we obtain (up to normalization depend-

ing on δ_x):

$$U_F^3 |\Psi_0\rangle \approx \left(|\Psi_0\rangle + e^{i\chi} |\Psi\rangle + e^{i\chi} |\tilde{\Psi}\rangle \right), \quad (9)$$

where $|\Psi\rangle, |\tilde{\Psi}\rangle$ are superpositions of states with zeros at every site except on two neighbouring sites, which contain a pair $+-$ or $-+$. Fixing the normalization constant for a total of $3n$ steps, this approach allows to obtain an approximate expression for the thermalization time scale, identified at the point where the overlap of the time evolved state respect to $|\Psi_0\rangle$ has value $1/2$. The total number of steps needed to reach that value in the overlap can be estimated to be the integer part of (see Supplemental Information for a detailed derivation):

$$\begin{aligned} n_t &\sim \frac{\log(1 - \eta^2) - \log(1 + \eta^2 - 2\eta \cos(\chi))}{\log \eta^2}, \\ \eta &= \frac{1}{\sqrt{1 + 2L\delta_x^2}}, \quad \chi = \frac{9\theta_z}{2}. \end{aligned} \quad (10)$$

Some maxima and minima for this function are identified at:

$$\chi = m\pi \quad m \in \mathbb{Z}. \quad (11)$$

In particular, for $m = 0, 2, 4$ one obtains minima values of this function, corresponding to $\theta_z = 0, \frac{4\pi}{9}, \frac{8\pi}{9}$, respectively. The points $\theta_z = \frac{4\pi}{9}, \frac{8\pi}{9}$ are in agreement with two of the dips observed in all phase diagrams at very small kick values of θ_x . The dip at $\theta_z = \frac{6\pi}{9}$ corresponds to the case $m = 3$. Given that the perturbative treatment identifies this point as a maxima rather than a minima, we argue that this point might originate from higher-order corrections.

ACKNOWLEDGEMENTS

This research was funded by the European Research Council (ERC, QUDITS, 101080086). Views and opinions expressed are however those of the author(s) only and do not necessarily reflect those of the European Union or the European Research Council Executive Agency. Neither the European Union nor the granting authority can be held responsible for them. We also acknowledge support by the Austrian Science Fund (FWF) through the SFB BeyondC (FWF Project No. F7109) and the EU-QUANTERA project TNiSQ (N-6001), and by the IQI GmbH. The authors gratefully acknowledge the scientific support and HPC resources provided by the German Aerospace Center (DLR). The HPC system CARO is partially funded by "Ministry of Science and Culture of Lower Saxony" and "Federal Ministry for Economic Affairs and Climate Action".

- [1] D. N. Basov, R. D. Averitt, and D. Hsieh, Towards properties on demand in quantum materials, *Nature Materials* **16**, 1077 (2017).
- [2] R. Moessner and S. L. Sondhi, Equilibration and order in quantum floquet matter, *Nature Physics* **13**, 424 (2017).
- [3] T. Oka and S. Kitamura, Floquet engineering of quantum materials, *Annual Review of Condensed Matter Physics* **10**, 387 (2019).
- [4] M. S. Rudner and N. H. Lindner, Band structure engineering and non-equilibrium dynamics in floquet topological insulators, *Nature Reviews Physics* **2**, 229 (2020).
- [5] A. Polkovnikov, K. Sengupta, A. Silva, and M. Vengalattore, Colloquium: Nonequilibrium dynamics of closed interacting quantum systems, *Rev. Mod. Phys.* **83**, 863 (2011).
- [6] L. D'Alessio and M. Rigol, Long-time behavior of isolated periodically driven interacting lattice systems, *Phys. Rev. X* **4**, 041048 (2014).
- [7] P. Ponte, A. Chandran, Z. Papić, and D. A. Abanin, Periodically driven ergodic and many-body localized quantum systems, *Annals of Physics* **353**, 196 (2015).
- [8] J. M. Deutsch, Quantum statistical mechanics in a closed system, *Phys. Rev. A* **43**, 2046 (1991).
- [9] M. Srednicki, Chaos and quantum thermalization, *Phys. Rev. E* **50**, 888 (1994).
- [10] M. Rigol, V. Dunjko, and M. Olshanii, Thermalization and its mechanism for generic isolated quantum systems, *Nature* **452**, 854 (2008).
- [11] H. Bernien, S. Schwartz, A. Keesling, H. Levine, A. Omran, H. Pichler, S. Choi, A. S. Zibrov, M. Endres, M. Greiner, V. Vuletić, and M. D. Lukin, Probing many-body dynamics on a 51-atom quantum simulator, *Nature* **551**, 579 (2017).
- [12] C. J. Turner, A. A. Michailidis, D. A. Abanin, M. Serbyn, and Z. Papić, Weak ergodicity breaking from quantum many-body scars, *Nature Physics* **14**, 745 (2018).
- [13] W. W. Ho, S. Choi, H. Pichler, and M. D. Lukin, Periodic orbits, entanglement, and quantum many-body scars in constrained models: Matrix product state approach, *Phys. Rev. Lett.* **122**, 040603 (2019).
- [14] S. Choi, C. J. Turner, H. Pichler, W. W. Ho, A. A. Michailidis, Z. Papić, M. Serbyn, M. D. Lukin, and D. A. Abanin, Emergent $su(2)$ dynamics and perfect quantum many-body scars, *Phys. Rev. Lett.* **122**, 220603 (2019).
- [15] Schechter2019, Weak ergodicity breaking and quantum many-body scars in spin-1 xy magnets, *Phys. Rev. Lett.* **123**, 147201 (2019).
- [16] M. Serbyn, D. A. Abanin, and Z. Papić, Quantum many-body scars and weak breaking of ergodicity, *Nature Physics* **17**, 675 (2021).
- [17] A. Chandran, T. Iadecola, V. Khemani, and R. Moessner, Quantum many-body scars: A quasiparticle perspective, *Annual Review of Condensed Matter Physics* **14**, 443 (2023).
- [18] P. W. Anderson, Absence of diffusion in certain random lattices, *Phys. Rev.* **109**, 1492 (1958).
- [19] I. V. Gornyi, A. D. Mirlin, and D. G. Polyakov, Interacting electrons in disordered wires: Anderson localization and low- t transport, *Phys. Rev. Lett.* **95**, 206603 (2005).
- [20] D. Basko, I. Aleiner, and B. Altshuler, Metal-insulator transition in a weakly interacting many-electron system with localized single-particle states, *Annals of Physics* **321**, 1126 (2006).
- [21] R. Nandkishore and D. A. Huse, Many-body localization and thermalization in quantum statistical mechanics, *Annual Review of Condensed Matter Physics* **6**, 15 (2015).
- [22] P. Ponte, Z. Papić, F. m. c. Huveneers, and D. A. Abanin, Many-body localization in periodically driven systems, *Phys. Rev. Lett.* **114**, 140401 (2015).
- [23] V. Khemani, A. Lazarides, R. Moessner, and S. L. Sondhi, Phase structure of driven quantum systems, *Phys. Rev. Lett.* **116**, 250401 (2016).
- [24] D. V. Else, B. Bauer, and C. Nayak, Floquet time crystals, *Phys. Rev. Lett.* **117**, 090402 (2016).
- [25] J. Zhang, P. W. Hess, A. Kyprianidis, P. Becker, A. Lee, J. Smith, G. Pagano, I.-D. Potirniche, A. C. Potter, A. Vishwanath, N. Y. Yao, and C. Monroe, Observation of a discrete time crystal, *Nature* **543**, 217 (2017).
- [26] S. Choi, J. Choi, R. Landig, G. Kucsko, H. Zhou, J. Isoya, F. Jelezko, S. Onoda, H. Sumiya, V. Khemani, C. von Keyserlingk, N. Y. Yao, E. Demler, and M. D. Lukin, Observation of discrete time-crystalline order in a disordered dipolar many-body system, *Nature* **543**, 221 (2017).
- [27] M. Ippoliti, K. Kechedzhi, R. Moessner, S. Sondhi, and V. Khemani, Many-body physics in the nisq era: Quantum programming a discrete time crystal, *PRX Quantum* **2**, 030346 (2021).
- [28] X. Mi, M. Ippoliti, C. Quintana, A. Greene, Z. Chen, J. Gross, F. Arute, K. Arya, J. Atalaya, R. Babush, J. C. Bardin, J. Basso, A. Bengtsson, A. Bilmes, A. Bourassa, L. Brill, M. Broughton, B. B. Buckley, D. A. Buell, B. Burkett, N. Bushnell, B. Chiaro, R. Collins, W. Courtney, D. Debroy, S. Demura, A. R. Derk, A. Dunsworth, D. Eppens, C. Erickson, E. Farhi, A. G. Fowler, B. Foxen, C. Gidney, M. Giustina, M. P. Harrigan, S. D. Harrington, J. Hilton, A. Ho, S. Hong, T. Huang, A. Huff, W. J. Huggins, L. B. Ioffe, S. V. Isakov, J. Iveland, E. Jeffrey, Z. Jiang, C. Jones, D. Kafri, T. Khattar, S. Kim, A. Kitaev, P. V. Klimov, A. N. Korotkov, F. Kostritsa, D. Landhuis, P. Laptev, J. Lee, K. Lee, A. Locharla, E. Lucero, O. Martin, J. R. McClean, T. McCourt, M. McEwen, K. C. Miao, M. Mohseni, S. Montazeri, W. Mruczkiewicz, O. Naaman, M. Neeley, C. Neill, M. Newman, M. Y. Niu, T. E. O'Brien, A. Opremcak, E. Ostby, B. Pato, A. Petukhov, N. C. Rubin, D. Sank, K. J. Satzinger, V. Shvarts, Y. Su, D. Strain, M. Szalay, M. D. Trevithick, B. Villalonga, T. White, Z. J. Yao, P. Yeh, J. Yoo, A. Zalcman, H. Neven, S. Boixo, V. Smelyanskiy, A. Megrant, J. Kelly, Y. Chen, S. L. Sondhi, R. Moessner, K. Kechedzhi, V. Khemani, and P. Roushan, Time-crystalline eigenstate order on a quantum processor, *Nature* **601**, 531 (2022).
- [29] P. Frey and S. Rachel, Realization of a discrete time crystal on 57 qubits of a quantum computer, *Science Advances* **8**, eabm7652 (2022).
- [30] J. Rovny, R. L. Blum, and S. E. Barrett, Observation of discrete-time-crystal signatures in an ordered dipolar many-body system, *Phys. Rev. Lett.* **120**, 180603 (2018).
- [31] P. Peng, C. Yin, X. Huang, C. Ramanathan, and P. Cappellaro, Floquet prethermalization in dipolar spin chains, *Nature Physics* **17**, 444 (2021).

- [32] J. Choi, H. Zhou, S. Choi, R. Landig, W. W. Ho, J. Isoya, F. Jelezko, S. Onoda, H. Sumiya, D. A. Abanin, and M. D. Lukin, Probing quantum thermalization of a disordered dipolar spin ensemble with discrete time-crystalline order, *Phys. Rev. Lett.* **122**, 043603 (2019).
- [33] J. Choi, H. Zhou, H. S. Knowles, R. Landig, S. Choi, and M. D. Lukin, Robust dynamic hamiltonian engineering of many-body spin systems, *Phys. Rev. X* **10**, 031002 (2020).
- [34] W. Beatrez, O. Janes, A. Akkiraju, A. Pillai, A. Oddo, P. Reshetikhin, E. Druga, M. McAllister, M. Elo, B. Gilbert, D. Suter, and A. Ajoy, Floquet prethermalization with lifetime exceeding 90 s in a bulk hyperpolarized solid, *Phys. Rev. Lett.* **127**, 170603 (2021).
- [35] B. Fauseweh, Quantum many-body simulations on digital quantum computers: State-of-the-art and future challenges, *Nature Communications* **15**, 2123 (2024).
- [36] M. Ringbauer, M. Meth, L. Postler, R. Stricker, R. Blatt, P. Schindler, and T. Monz, A universal qudit quantum processor with trapped ions, *Nature Physics* **18**, 1053 (2022).
- [37] T. c. v. Prosen, Time evolution of a quantum many-body system: Transition from integrability to ergodicity in the thermodynamic limit, *Phys. Rev. Lett.* **80**, 1808 (1998).
- [38] L. D'Alessio and A. Polkovnikov, Many-body energy localization transition in periodically driven systems, *Annals of Physics* **333**, 19 (2013).
- [39] D. A. Abanin, W. De Roeck, and F. m. c. Huveneers, Exponentially slow heating in periodically driven many-body systems, *Phys. Rev. Lett.* **115**, 256803 (2015).
- [40] D. V. Else, B. Bauer, and C. Nayak, Prethermal phases of matter protected by time-translation symmetry, *Phys. Rev. X* **7**, 011026 (2017).
- [41] W. W. Ho, T. Mori, D. A. Abanin, and E. G. Dalla Torre, Quantum and classical floquet prethermalization, *Annals of Physics* **454**, 169297 (2023).
- [42] T. Mori, T. N. Ikeda, E. Kaminishi, and M. Ueda, Thermalization and prethermalization in isolated quantum systems: a theoretical overview, *Journal of Physics B: Atomic, Molecular and Optical Physics* **51**, 112001 (2018).
- [43] K. Mallayya, M. Rigol, and W. De Roeck, Prethermalization and thermalization in isolated quantum systems, *Phys. Rev. X* **9**, 021027 (2019).
- [44] D. J. Luitz, R. Moessner, S. L. Sondhi, and V. Khemani, Prethermalization without temperature, *Phys. Rev. X* **10**, 021046 (2020).
- [45] L. Pezzè, A. Smerzi, M. K. Oberthaler, R. Schmied, and P. Treutlein, Quantum metrology with nonclassical states of atomic ensembles, *Rev. Mod. Phys.* **90**, 035005 (2018).
- [46] P. Hauke, M. Heyl, L. Tagliacozzo, and P. Zoller, Measuring multipartite entanglement through dynamic susceptibilities, *Nature Physics* **12**, 778 (2016).
- [47] G. Gyawali, T. Cochran, Y. Lensky, E. Rosenberg, A. H. Karamlou, K. Kechedzhi, J. Berndtsson, T. Westerhout, A. Asfaw, D. Abanin, R. Acharya, L. A. Beni, T. I. Andersen, M. Ansmann, F. Arute, K. Arya, N. Astrakhantsev, J. Atalaya, R. Babbush, B. Ballard, J. C. Bardin, A. Bengtsson, A. Bilmes, G. Bortoli, A. Bourassa, J. Bovaird, L. Brill, M. Broughton, D. A. Browne, B. Buchea, B. B. Buckley, D. A. Buell, T. Burger, B. Burkett, N. Bushnell, A. Cabrera, J. Campero, H.-S. Chang, Z. Chen, B. Chiaro, J. Claes, A. Y. Cleland, J. Cogan, R. Collins, P. Conner, W. Courtney, A. L. Crook, S. Das, D. M. Debroy, L. D. Lorenzo, A. D. T. Barba, S. Demura, A. D. Paolo, P. Donohoe, I. Drozdov, A. Dunsworth, C. Earle, A. Eickbusch, A. M. Elbag, M. Elzouka, C. Erickson, L. Faoro, R. Fatemi, V. S. Ferreira, L. F. Burgos, E. Forati, A. G. Fowler, B. Foxen, S. Ganjam, R. Gasca, W. Giang, C. Gidney, D. Gilboa, R. Gosula, A. G. Dau, D. Graumann, A. Greene, J. A. Gross, S. Habegger, M. C. Hamilton, M. Hansen, M. P. Harrigan, S. D. Harrington, S. Heslin, P. Heu, G. Hill, J. Hilton, M. R. Hoffmann, H.-Y. Huang, A. Huff, W. J. Huggins, L. B. Ioffe, S. V. Isakov, E. Jeffrey, Z. Jiang, C. Jones, S. Jordan, C. Joshi, P. Juhas, D. Kafri, H. Kang, T. Khaira, T. Khattar, M. Khezri, M. Kieferová, S. Kim, P. V. Klimov, A. R. Klots, B. Kobrin, A. N. Korotkov, F. Kostritsa, J. M. Kreikebaum, V. D. Kurilovich, D. Landhuis, T. Lange-Dei, B. W. Langley, P. Laptev, K.-M. Lau, L. L. Guevel, J. Ledford, J. Lee, K. Lee, B. J. Lester, W. Y. Li, A. T. Lill, W. Liu, W. P. Livingston, A. Locharla, D. Lundahl, A. Lunt, S. Madhuk, A. Maloney, S. Mandrà, L. S. Martin, S. Martin, O. Martin, C. Maxfield, J. R. McClean, M. McEwen, S. Meeks, A. Megrant, X. Mi, K. C. Miao, A. Mieszala, S. Molina, S. Montazeri, A. Morvan, R. Movassagh, C. Neill, A. Nersisyan, M. Newman, A. Nguyen, M. Nguyen, C.-H. Ni, M. Y. Niu, W. D. Oliver, K. Ottosson, A. Pizzuto, R. Potter, O. Pritchard, L. P. Pryadko, C. Quintana, M. J. Reagor, D. M. Rhodes, G. Roberts, C. Rocque, N. C. Rubin, N. Saei, K. Sankaragomathi, K. J. Satzinger, H. F. Schurkus, C. Schuster, M. J. Shearn, A. Shorter, N. Shutty, V. Shvarts, V. Sivak, J. Skrzuzny, S. Small, W. C. Smith, S. Springer, G. Sterling, J. Suchard, M. Szalay, A. Szasz, A. Szein, D. Thor, M. M. Torunbalci, A. Vaishnav, S. Vdovichev, G. Vidal, C. V. Heidweiller, S. Waltman, S. X. Wang, T. White, K. Wong, B. W. K. Woo, C. Xing, Z. J. Yao, P. Yeh, B. Ying, J. Yoo, N. Yosri, G. Young, A. Zalcman, Y. Zhang, N. Zhu, N. Zobrist, S. Boixo, J. Kelly, E. Lucero, Y. Chen, V. Smelyanskiy, H. Neven, D. Kovrizhin, J. Knolle, J. C. Halimeh, I. Aleiner, R. Moessner, and P. Roushan, Observation of disorder-free localization and efficient disorder averaging on a quantum processor (2024), arXiv:2410.06557 [quant-ph].
- [48] G. Camacho and B. Fauseweh, Prolonging a discrete time crystal by quantum-classical feedback, *Phys. Rev. Res.* **6**, 033092 (2024).
- [49] G. Tóth, Multipartite entanglement and high-precision metrology, *Phys. Rev. A* **85**, 022322 (2012).
- [50] D. R. Baykusheva, M. H. Kalthoff, D. Hofmann, M. Claassen, D. M. Kennes, M. A. Sentef, and M. Mitra, Witnessing nonequilibrium entanglement dynamics in a strongly correlated fermionic chain, *Phys. Rev. Lett.* **130**, 106902 (2023).
- [51] J. Smith, A. Lee, P. Richerme, B. Neyenhuis, P. W. Hess, P. Hauke, M. Heyl, D. A. Huse, and C. Monroe, Many-body localization in a quantum simulator with programmable random disorder, *Nature Physics* **12**, 907 (2016).
- [52] M. P. Fisher, V. Khemani, A. Nahum, and S. Vijay, Random quantum circuits, *Annual Review of Condensed Matter Physics* **14**, 335 (2023).
- [53] G. Vidal, Efficient classical simulation of slightly entangled quantum computations, *Phys. Rev. Lett.* **91**, 147902 (2003).